


Article

Winter Climate of Northeastern Dominican Republic and Cash Crop Production

Mark R. Jury ^{1,2} 

¹ Physics Department, University of Puerto Rico Mayagüez, Mayagüez PR 00681, Puerto Rico; mark.jury@upr.edu

² Geography Department, University of Zululand, KwaDlangezwa 3886, South Africa

Abstract: The winter climate of the northeastern Dominican Republic features steady rainfall, which sustains cash crop production. Using a representative season, December 2016–February 2017, the mesoscale climate is characterized by high-resolution reanalysis, satellite measurements and local observations, and statistical analyses of time series from an index area of 18.8–19.6° N, 70.4–69.6° W in the Cibao Valley, where cacao and coffee are grown. Winter rainfall depends on strong trade winds that push shallow stratiform convections over 100 km inland, where nocturnal drainage flows induce orographic uplift. Interannual climate variability is studied in the context of cacao and coffee production in the years 1976–2019. Lag correlations demonstrate that higher yields follow a wet autumn, a windy winter with cool sea temperatures, and a dry spring. Changes in high-value agricultural production in the northeastern Dominican Republic may be anticipated by the climatic determinants uncovered here.

Keywords: Dominican Republic; mesoscale circulation; winter trade wind rains

1. Introduction

1.1. Background Geography and Climate

The central Antilles island of Hispanola, with a surface area of 76 K km², lies in the prevailing trade winds and has mountain ridges exceeding 2000 m elevation that are densely vegetated. The sea surface temperatures (SSTs) along the Atlantic coast are ~27 °C during the winter, and subsidence by the Hadley cell keeps the marine layer shallow and neutrally stable. The hydrology of the Dominican Republic supports farming outputs of USD 10 billion and a population of 10+ million via wet spells from tropical troughs in the summer and orographic convection in the winter. Hydro-electric power exceeds 600 MW in the country, with the largest reservoir on the Yuna River at 19° N, 70.2° W [1]. The mesoscale structure and meteorological forcing of the summer climate have received attention [2]; less is known of the processes underpinning the winter climate. High-resolution data assimilation products can be employed to understand thermal-orographic circulations over the Antilles Islands and their consequences for agricultural resources, extending the earlier work of Perez and Jury [3], which analyzed long-term trends.

Garcia et al. [4] found that intensified trade winds promote orographic lifting on the northeast flank of Hispaniola; frontal intrusions contributed 40% of the winter rainfall. Dry and wet cases were distinguished by [4] using a composite analysis. The wet weather was related to a stronger anticyclone ridge southeast of Florida and deeper moisture advection from the Atlantic. Field surveys in the highlands [5] found winter mean nocturnal temperatures of 12 °C at elevations of 1500 m, and a persistent trade wind inversion at ~2200 m capped by a humidity < 40%, which only weakens during the infrequent passage of troughs.



Citation: Jury, M.R. Winter Climate of Northeastern Dominican Republic and Cash Crop Production. *Climate* **2023**, *11*, 161. <https://doi.org/10.3390/cli11080161>

Academic Editors: Timothy G. F. Kittel and Nir Y. Krakauer

Received: 22 April 2023

Revised: 6 July 2023

Accepted: 19 July 2023

Published: 27 July 2023



Copyright: © 2023 by the author. Licensee MDPI, Basel, Switzerland. This article is an open access article distributed under the terms and conditions of the Creative Commons Attribution (CC BY) license (<https://creativecommons.org/licenses/by/4.0/>).

1.2. Local Uptake of Climate Change

Izzo et al. [6] found little trend in the long-term rainfall over the northeastern Dominican Republic, likely associated with the opposing effects of increased surface humidity and subsident northerly winds, as noted in [7]. Climate change studies reveal steady warming but mixed hydrological outcomes: drying trends over the coastal lowlands in coarse-resolution model projections and moistening trends over the windward mountains in fine-resolution hindcasts [8,9]. Of some concern are the multi-year dry spells (1989–1991, 2001–2003, 2014–2015, 2018–2019) that induce water scarcity and lost crop production [10].

1.3. Importance of Agriculture in the Dominican Republic

Agriculture accounts for ~50% of land use, >75% of water use, and contributes 12% of country-level economic production [1]; nearly half is concentrated in the Cibao Valley and adjoining foothills (Figure 1A). At lower elevations of the eastern Yuna catchment, rice production is dominant, whereas cash crop farming is prevalent at higher elevations. The authors of [11,12] review the climate sensitivity of cacao, indicating crop preference for sunny weather, mean temperatures above 24 °C, and rainfall above 1200 mm/yr, but they also cite phenological inhibition by drought and flood. During cocoa production, sunny weather is critical for fermentation [13]. Coffee is grown at higher elevations and shows preference for mean temperatures below 24 °C and cloudy weather with rainfall above 1200 mm/yr [14–16]. Both crops are prone to diseases and pests when the climate is out of range for successive months. Although production losses follow intense hurricanes such as Georges 1998, most cacao and coffee plantations in the Dominican Republic are sheltered by coastal mountains. Cacao/coffee production trends are upward/downward, respectively, but multi-year fluctuations of yield and economic value are coherent [17,18] and justify country-level analysis.

1.4. Objectives and Preface

The main objectives of this study are to (i) characterize the mesoscale winter climate of the Dominican Republic for a representative season (December 2016–February 2017); (ii) understand diurnal cycles and boundary layer responses under trade wind airflow; (iii) identify the processes driving nocturnal convection on windward slopes; and (iv) evaluate the sensitivity of cacao and coffee yields to climate variability. To achieve these objectives, mesoscale reanalyses that assimilate local observations and satellite data are employed. In Section 2, the methods of data analysis are reviewed. Section 3 gives the results that are sub-divided into representative climate, diurnal and case features, and crop sensitivity. Section 4 provides a summarizing discussion. This work is novel in using high-resolution reanalysis and satellite products to describe the winter climate of the Dominican Republic and uncovering the links between regional climate variability, local winds and rainfall, and cacao and coffee production in the Cibao Valley.

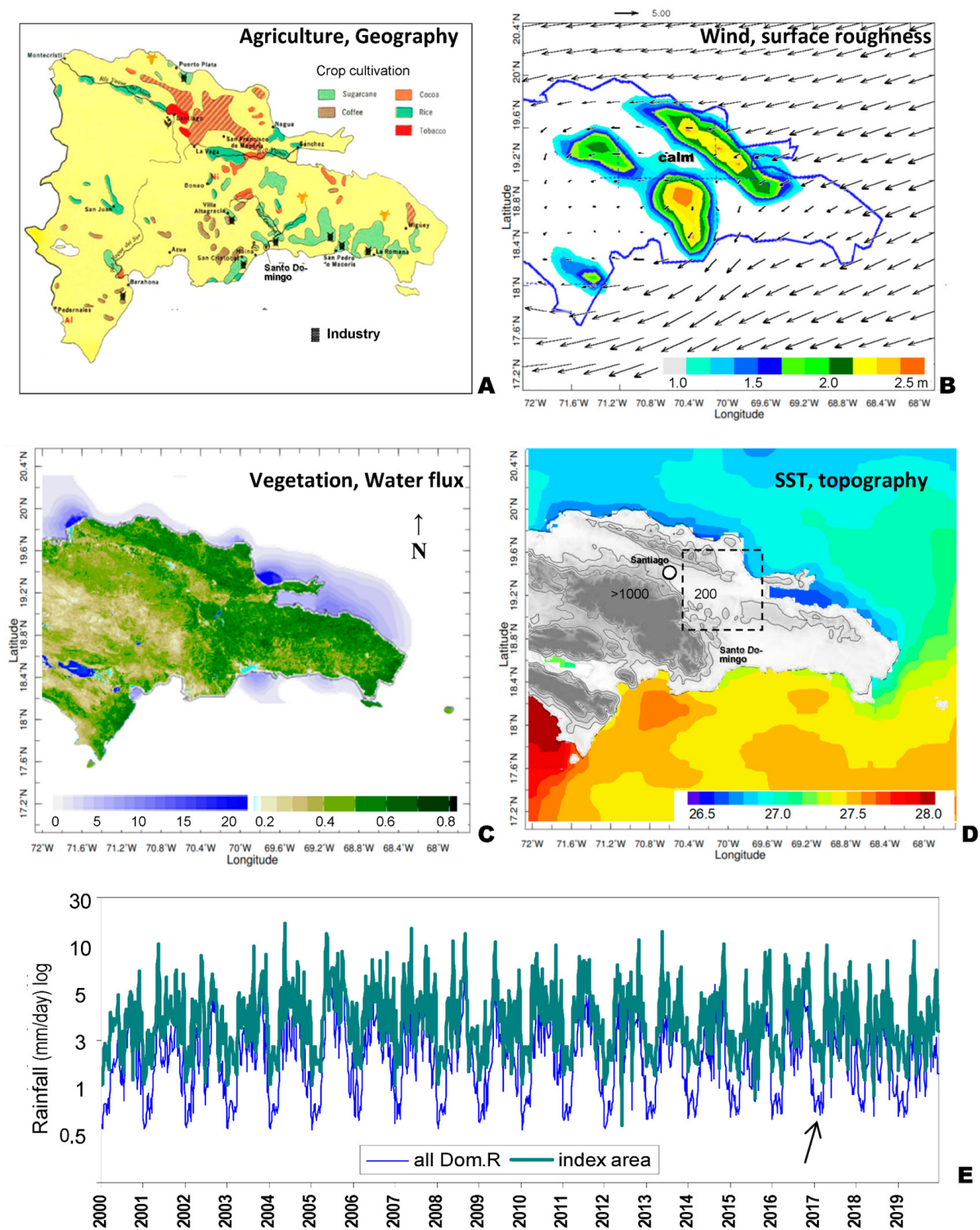


Figure 1. Maps of Dominican Republic: (A) agricultural and economic activity, (B) DJF17 ERA5 wind vectors (m/s) and NAM surface roughness (m, shaded), (C) DJF17 MODIS VIS land color (% fraction, green) and HYCOM water flux to sea (mm/day, blue), and (D) DJF17 MODIS IR sea surface temperature ((C), shaded), with elevation gray scale contours (m). (E) Temporal record of daily rainfall over Dominican Republic with arrow pointing to DJF17 season, comparing country-wide and northeastern index area. Hatched in (A) refers to coffee and cocoa production area; yellow is background land. Dashed box in (D) is the index area used for temporal analysis; circle is the Santiago airport.

2. Data and Methods

The Dominican Republic has a dense weather station network [19] and regular AM-DAR aircraft profiles (at Santiago, 19.4° N, 70.6° W), which are assimilated with satellite data into reanalyses. Rainfall patterns are derived from two high-resolution multi-satellite products: CHIRP and GPM [20,21]. Atmospheric conditions are characterized by three mesoscale reanalyses: CFSr2, ERA5, and NAM [22–24]. Oceanographic patterns are studied via HYCOM and W3 [25,26]. Land surface conditions are described by NOAA satellite visible color (vegetation fraction) and infrared temperature. The surface ocean around the Dominican Republic is analyzed for SST, evaporation, and water fluxes. The gridded products have 5–25 km of horizontal resolution and 1–24 h of time resolution, as described by Table 1 with acronyms. The CFSr2 and ERA5 reanalyses are ensemble-averaged to increase confidence in the results, while high-resolution NAM reanalysis and CHIRP rainfall are used in case studies.

Table 1. Data acronyms, definitions, and resolution.

Acronym	Name and Variable	Space and Time Resolution
CFSr2	Coupled Forecast System reanalysis v2 thermodynamic and circulation parameters	25 km, hourly
CHIRP	Climate Hazards InfraRed Precipitation geostationary IR satellite	5 km, daily
CloudSat	CALIPSO cloud radar slice microwave reflectivity	1 km, weekly
CRU4	Climate Research Univ v4 rainfall interpolated gauges (land)	25 km, monthly
ENSO NAO	El Nino Southern Oscillation (Pacific) North Atlantic Oscillation climate index	area, monthly
ERA5	European Centre for Medium-Range Weather Forecasts reanalysis v5	25 km, hourly
FAO	Food and Agriculture Organization crop production (cacao and coffee)	country, yearly
GPM	Global Precipitation Monitoring IR and MW multi-satellite	10 km, hourly
HYCOM	Hybrid Coordinate Ocean Model v3 heat and water flux (sea)	10 km, daily
MODIS	Moderate-imaging Infrared Spectrometer, land surface temp., and vegetation color	5 km, weekly
NAM	North American Mesoscale model with WRF data assimilation	10 km, 3 hourly
net OLR	Outgoing Longwave Radiation satellite proxy for cloudiness	25 km, daily
Station	Santiago airport wind, temp., and aircraft observations	point, hourly
W3	Wave-watch v3 reanalysis sea state characteristics	25 km, 3 hourly

Following an evaluation of winter season anomalies for surface wind, rainfall, and SST, December 2016–February 2017 (hereafter DJF17) was used to represent the mesoscale climate in the domain: 17–20.5° N, 72.0–67.75° W. Its departures from long-term mean are $<0.1\sigma$. Temporal analyses are drawn from an index area: 18.8–19.6° N, 70.4–69.6° W comprising the eastern Cibao Valley and Yuna River catchment, an agriculturally productive zone (Figure 1A), especially for cacao and coffee.

The index area mean diurnal cycle was calculated from hourly time series in DJF17 ($N = 2160$) for GPM rainfall, zonal wind speed, sensible heat flux, and related parameters from CFSr2 and ERA5 reanalyses. Index area GPM rainfall from midnight to sunrise was ranked, and the top cases were selected for study: 24 December 2016, 27 December 2016, 1 January 2017, 9 January 2017, 16 January 2017, and 12 February 2017 (Table 2). Santiago airport AMDAR wind and temperature profiles at 09:00 for these nocturnal rainfall cases were compared. NAM wind streamline patterns were analyzed for three case days and a CloudSat reflectivity slice was obtained. Vertical cross-sections of the low level circulation were analyzed, and scatterplots of index area hourly zonal wind and surface temperature in DJF17 were made, $N = 2160$.

Table 2. Highest-ranked cases of 00:00–08:00 hr GPM rainfall (mm/h) and accompanying ERA5 zonal wind (m/s) averaged over the index area, with local time of peak rainfall listed.

Date	Hour	Rain	U Wind
24 December 2016	07:00	1.47	−4.2
27 December 2016	03:00	1.86	−4.9
1 January 2017	06:00	0.87	−5.2
9 January 2017	07:00	1.06	−2.4
16 January 2017	06:00	1.22	−4.7
12 February 2017	08:00	0.98	−3.4

Having analyzed a representative winter for mesoscale climate patterns, the second component of the research focuses on temporal analyses via point-to-field regression of detrended annual FAO cacao–coffee yields in the Dominican Republic 1976–2019 onto regional maps of Hadley SST, ERA5 200 hPa zonal wind and NOAA satellite net OLR (proxy for cloudiness). Yields were also regressed onto local fields of detrended ERA5 surface zonal (U) wind and net solar radiation ($N > 42$). Insignificant field regressions were masked. Temporal lag correlations were calculated between the detrended cacao–coffee yields and monthly climate parameters averaged over the Cibao Valley index area of 1976–2019, wherein December–February season emerged as most influential. Spatial regression fields and lag correlation significance above 95% confidence requires $r > |0.26|$ with ~ 40 degrees of freedom due to annual cycling. Pearson product-moment lag correlations use monthly time series that tend to be normally distributed, as seen in the Appendix A. Outcomes evolve into three parts: (i) analysis of a representative mean winter climate, (ii) case study of winter trade winds and diurnal cycling, and (iii) temporal statistics on inter-annual variability applied to detrended annual agricultural yields. Limitations of the study derive from uncertainties in national crop yield statistics reported to FAO. The reader will note in the acknowledgements that data and statistics are generated by freely available online resources.

3. Results

3.1. Winter Climate

Climatic patterns around the Dominican Republic are shown in Figure 1A–D. Crop cultivation is concentrated in the northeastern interior for cacao and coffee, while sugarcane is along the south coastal plains. The annual cycle of soil moisture in the eastern Cibao Valley (not shown) crests in October at above 70%. Drying is essential for crop production during the winter so that soil moisture approaches 50% by March. Trade winds surround the island during a representative winter (DJF17), but there is a calm area over the northeastern interior due to upstream roughness and nocturnal cooling that decouples the airflow (as shown below). The dry season vegetation fraction exceeds 0.5 in the northeast, in contrast with <0.3 in the leeward southwest. The DJF17 water flux to the sea exceeds 20 mm/month at river mouths in the northwest and northeast. Northeasterly trade winds flow over the island from the Atlantic, where SST are $<27^\circ\text{C}$ during the winter. The temporal record of daily rainfall in the period 2000–2019 (Figure 1E) oscillates from 1 mm/day in the dry

season to 10 mm/day in the wet season. Rainfall in the Cibao Valley is noticeably wetter than country-wide values during the winter but is similar in the summer.

The pattern of winter DJF17 rainfall is illustrated in Figure 3A based on the CFSr2-ERA5 ensemble and CHIRP products. There is a bow wave pattern of higher rainfall in a N-S swath along 70° W, extending seaward and crossing the south coast near Santo Domingo. The northeastern coastal mountains experienced orographic rainfall > 200 mm; elsewhere, the DJF17 winter totals were paltry. Rainfall pushes further inland in the CHIRP product compared with CFSr2-ERA5 reanalyses, likely due to its higher resolution. The vertical cross-section on 19.2° N (Figure 3B) reveals a deceleration of coastal trade winds that induces uplift over 70° W (San Francisco de Macoris). Diurnal analyses (Figure 3C,D) reveal how uplift relates to nocturnal cooling, as outlined below.

Sensible heat fluxes over the northeastern coastal plains are negative during the night and gradually decouple surface winds to a minimum near sunrise. The sensible heat flux rises slowly in the morning and reaches a diurnal peak near 14:00 hr. DJF17 mean nocturnal rainfall was ~0.07 mm/h (satellite) and ~0.12 mm/h (reanalysis) according to Figure 3C, constituting 29% (satellite) to 45% (reanalysis) of the seasonal total. Diurnal rain rate doubled to ~0.17 mm/h during midday heating accompanied by the sea breeze (−U wind in Figure 3D).

DJF17 mean minimum temperatures are analyzed in Figure 2A and reveal a cool 14–20 °C air mass over the highlands that extends coastward. Wind statistics from Santiago airport in the Cibao Valley are presented in Figure 2B and Table 3. Most of the winds are from 078 to 145° in the range 1–6 m/s; however, land breezes < 4 m/s from 258 to 347° are present, and calms are noted 29% of the time. The scatterplot of index area T and U is illustrated in Figure 2C, wherein lower temperatures correspond with nocturnal drainage flow (+U). Conversely, warmer temperatures initiate diurnal sea breezes, which intensify the trade winds (−U). Upstream from the index area, trade winds are 7 m/s (cf. Figure 1B). Thus, deceleration $\partial U / \partial x$ of -10^{-5} s^{-1} induces convergence and uplift over the index area, particularly from midnight to sunrise, when calms at Santiago are noted 57% of the time. The slowing trade winds (cf. Figure 3B) generate nocturnal rainfall, as seen below.

Table 3. Hourly % wind frequency distribution in DJF17 at Santiago airport, and percentage in column vs. row: speed class (m/s) vs. direction sector, with land breezes in bold (lower), sample size N ~2000; see Figure 2B.

Direction	1.0–1.9	2.0–2.9	3.0–3.9	4.0–5.9	6.0–7.9	8.0+ m/s
348–010°	0.24	0.59	0.30	0.12	0.06	0.00
011–032°	0.24	0.36	0.24	0.12	0.00	0.00
033–055°	0.53	0.65	0.06	0.24	0.06	0.00
056–077°	0.36	1.01	0.42	0.95	0.06	0.00
078–100°	0.53	3.56	2.85	2.85	1.19	0.00
101–122°	0.53	3.44	3.86	6.05	3.21	0.36
123–145°	0.42	4.21	3.50	4.10	1.48	0.24
146–167°	0.30	3.44	1.96	2.08	0.42	0.06
168–190°	0.42	1.72	0.59	0.36	0.06	0.00
191–212°	0.24	0.77	0.12	0.06	0.00	0.00
213–235°	0.18	0.77	0.00	0.00	0.00	0.00
236–257°	0.18	0.30	0.06	0.00	0.00	0.00
258–280°	0.18	0.71	0.18	0.06	0.00	0.00
281–302°	0.24	1.07	0.71	0.71	0.06	0.06
303–325°	0.24	0.83	0.36	0.59	0.18	0.06
326–347°	0.24	0.71	0.18	0.12	0.24	0.00
Calm	29.26					

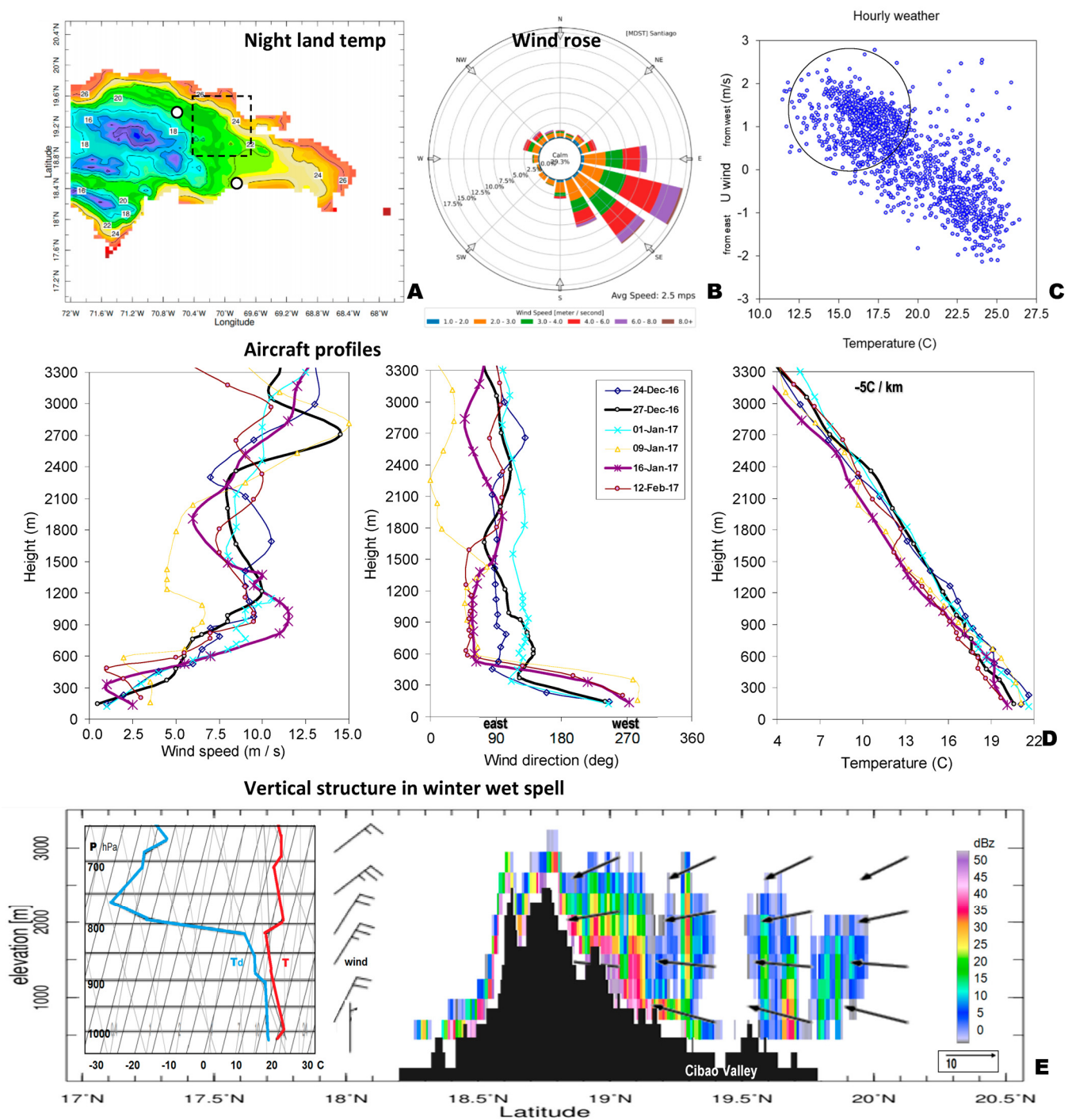


Figure 2. (A) MODIS nighttime land surface temperatures with index area (dashed box) and airports (dots), (B) DJF17 airport wind rose (cf. Table 3), and (C) scatterplot of hourly temperature vs. zonal wind ($N = 2160$), from CFSr2-ERA5 ensemble reanalysis with nocturnal land breezes circled. (D) AMDAR aircraft profiles at 09:00 hr from Santiago airport for cases listed in Table 2 (left-right: speed, direction, and temperature). (E) Cloudsat reflectivity slice on 70.4 W on 12 January 2017 with meridional circulation to north and Santo Domingo radiosonde profile to south.

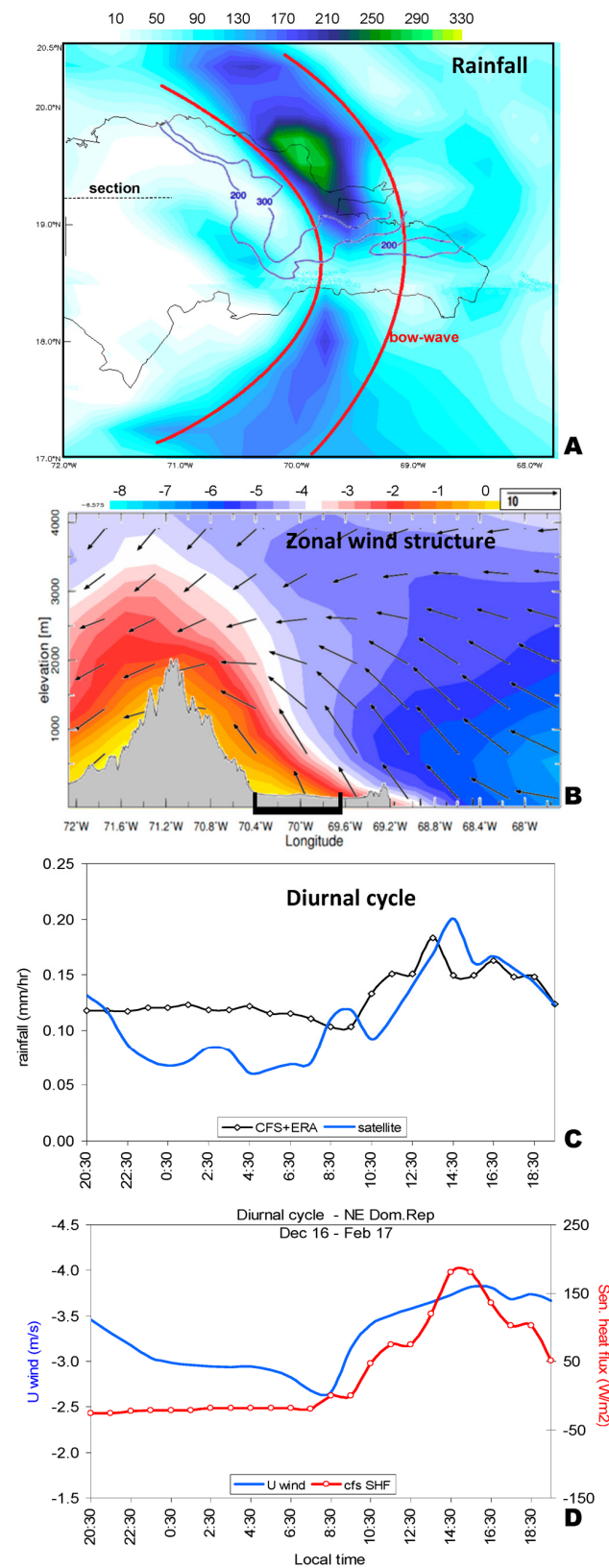


Figure 3. DJF17 mean: (A) map of total rainfall CFSr2-ERA5 ensemble average (mm, shaded) and CHIRP (contour > 200 mm) with schematic bow wave; (B) vertical cross-section on 19.2° N of ERA5 zonal wind (m/s, shaded) and circulation vectors (m/s, vertical motion exaggerated). Diurnal cycle for the index area: (C) rainfall; (D) meteorological parameters, N = 2160, where $-U$ wind refers to stronger trades (in the afternoon).

3.2. Case Features

Early morning Santiago aircraft profiles are shown in Figure 2D for the six highest-ranked nocturnal rainfall cases in DJF17 (cf. Table 2). Below 500 m, the wind speeds are < 2.5 m/s, and the wind directions are from 200 to 280° , reflecting air drainage from the highlands. Temperature profiles show a steady decline of $-5^\circ\text{C}/\text{km}$. Above 500 m, easterly flow is evident, and wind speeds increase to >7.5 m/s. Thus, nocturnal rainfall over the Cibao Valley is induced by drainage flow underlying the prevailing trade winds.

In Figure 2E, a CloudSat reflectivity slice is presented. High cloud droplet reflectivity is over windward slopes facing the incoming Atlantic circulation, which has a rising motion below 1000 m and a sinking motion above 2000 m. Stratiform convection is confined to the layer 500–2500 m and reaches 40 dBz north of mountains from 18.9 to 19.1° N and over the coastal range at 19.6° N. There is diminished reflectivity in the intervening Cibao Valley, where cacao and coffee are grown. The radiosonde profile at Santo Domingo (Figure 2E inset) reveals a moist layer to 2000 m, capped by an inversion within northeasterly airflow. From these results, the reader can infer that winter rainfall in the northeastern Dominican Republic is derived from shallow clouds and fueled by surface fluxes over the Atlantic Ocean.

NAM streamline analyses at 05:00 hr for three cases are illustrated in Figure 4A–C, accompanied by large-scale 500 hPa geopotential anomaly maps. There is a consistent pattern of marine trade winds interacting with drainage flow from the interior. Airflow is from 45 to 65° at 9 – 10 m/s, representing post-frontal conditions with an upper ridge to the northwest. A divergent land breeze spirals outward from the highlands and meets the Atlantic inflow over the Cibao Valley. The confluence induces stratiform rainfall between midnight and sunrise. This circulation recurs when a mid-latitude ridge joins the subtropical anticyclone, as illustrated by the case of 27 December 2016 (Figure 5A,B).

Large-scale wind and evaporation maps reflect the North Atlantic anticyclone driving moist airflow toward the Dominican Republic over 2000 km. Marine evaporation rates exceed 10 mm/day, consistent with post-frontal sea-to-air latent heat transfer. Steep ocean waves (Figure 5C–E) of 3 m height with a 9 s period from a 030° direction are accompanied by >10 m/s winds that deepen the marine layer to ~ 1000 m. Stratiform rainfall on 27 December 2016 (Figure 5F) was ~ 10 mm and extended 100 km inland over windward slopes. A back-trajectory analysis demonstrates that nocturnal airflow reaching the Cibao Valley is confined to a shallow layer (Figure 5G) that limits convection to lower elevations.

3.3. Interannual Climate Variability and Crop Yields

Statistical regressions of annual crop yields onto environmental fields provide an economic context for the climatologies above. The temporal record of value and yield is presented in Figure 6A, representing equal contributions from FAO cacao and coffee data for the Dominican Republic. Economic production values have declined since the 1990s, while yields show interannual periodicities of 2–3 and 5–6 years. The yields relate to the large-scale environment (Figure 6A–D) via cooler tropical Atlantic SST, reduced convection (+netOLR) extending from Panama, and upper westerly winds over the Caribbean. Together, these indicate that yields are enhanced when the climate stays in a phenological range and tropical cyclogenesis is suppressed by wind shear. Correlations with the El Niño Southern Oscillation (ENSO) were weak, but the North Atlantic Oscillation (NAO) yielded a +0.30 coefficient with respect to the cacao–coffee time series. Positive NAO coincides with mid-latitude ridging off the southeastern USA [27]. Climatic controls on cash crop production emerge from lag correlations (Figure 6F). Increased evapotranspiration in the autumn, stronger trade winds in the winter, and greater solar radiation in the spring (+0.31 at +2 months)—these climate parameters act to deplete soil moisture to a suitable phenological range. The influence of trade winds is steady from lag -5 to +2 months (September–March) and strong (-0.45), indicating that accelerated easterly winds during the winter season favors cacao and coffee production.

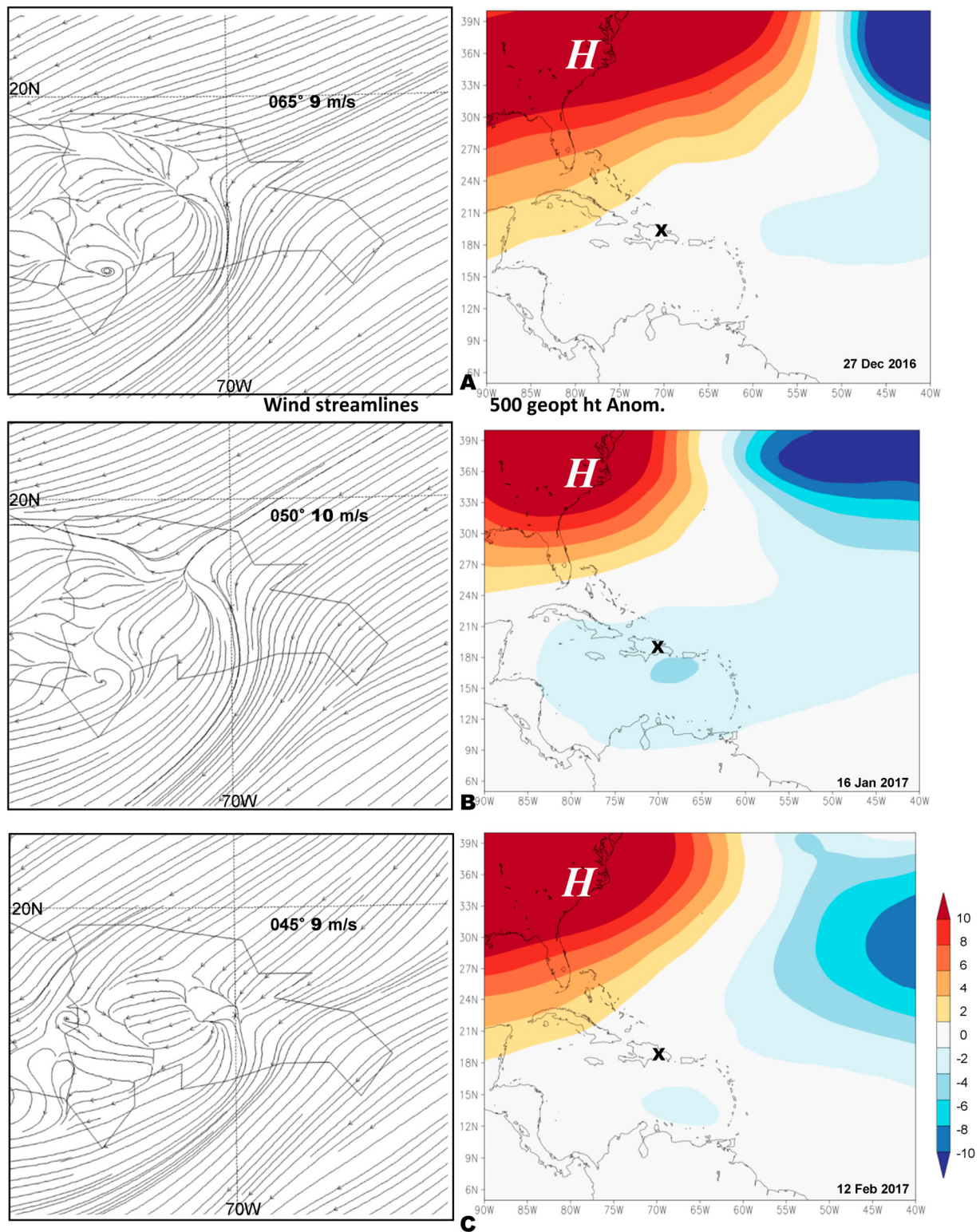


Figure 4. Nocturnal rainfall cases of NAM wind streamlines at 05:00 hr on (A) 27 December 2016, (B) 16 January 2017, and (C) 12 February 2017 with incoming marine trade winds labeled. Associated large-scale ERA5 500 hPa geopotential height anomalies (m, right) for the same days (x index area).

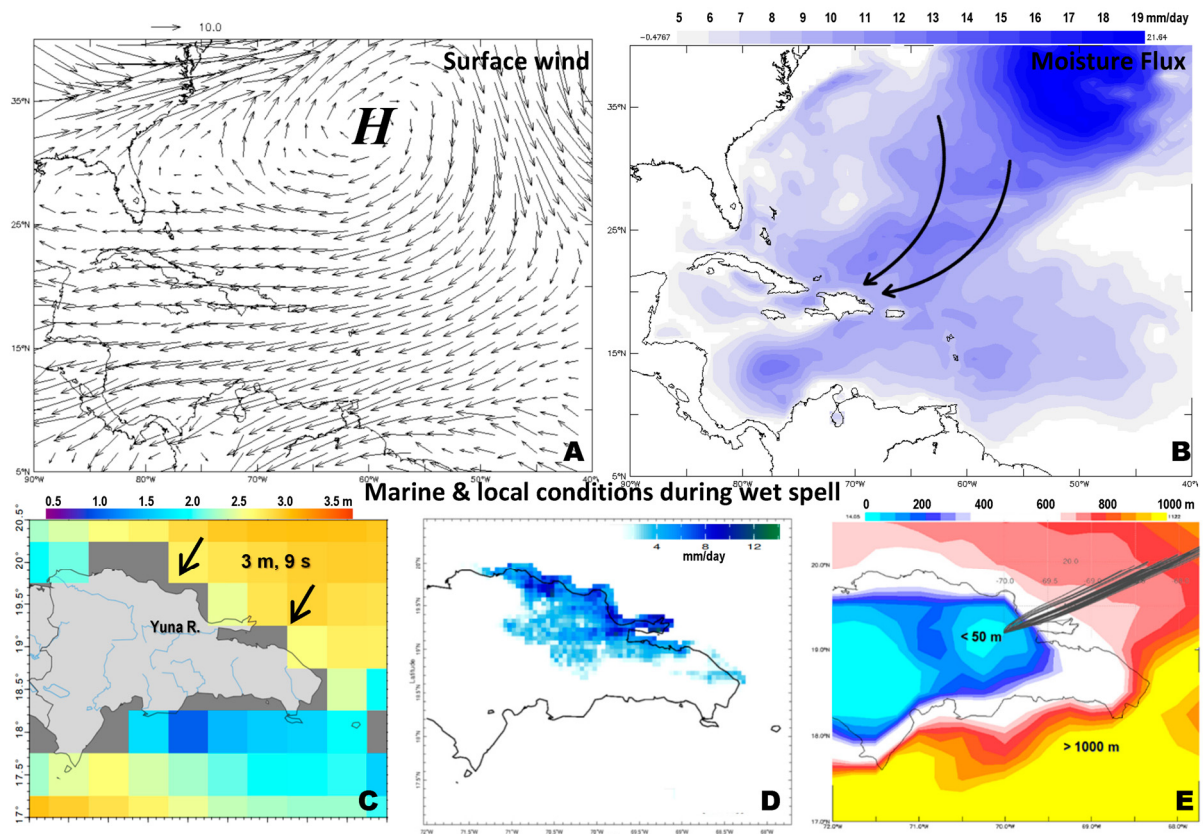


Figure 5. Case of 27 December 2016: (A,B) large-scale surface wind and evaporation maps, (C) regional wave height (shaded) with direction arrows and period, (D) daily CHIRP rainfall, and (E) nocturnal boundary layer height (shaded) with 00–08 hr back trajectories arriving at the index area. Arrows in (B) emphasize the 2000 km fetch producing the large waves in (C).

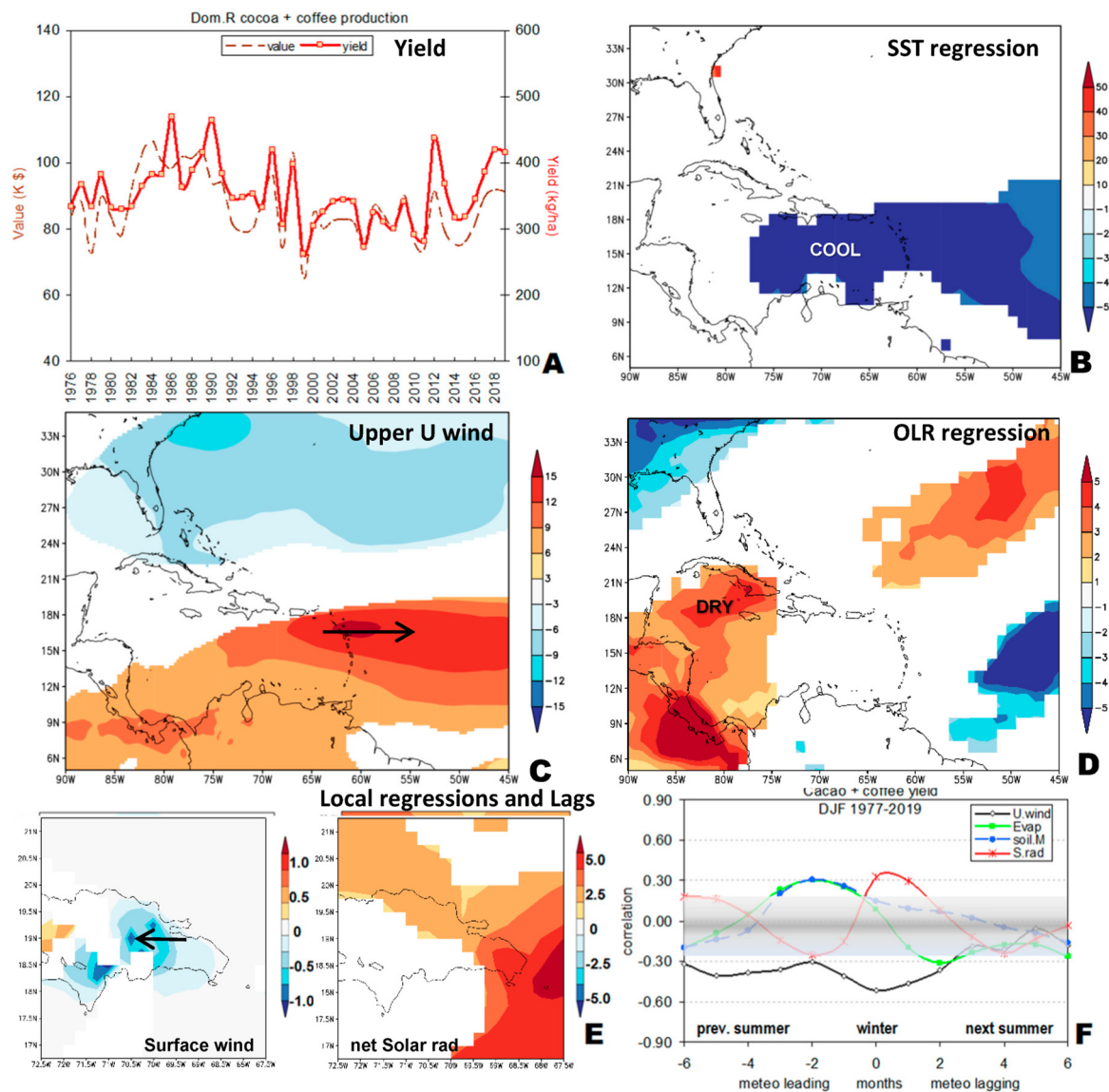


Figure 6. (A) Dominican Republic cacao–coffee annual production value and yield record. Regression of detrended annual cacao–coffee yield (1976–2019) onto large-scale fields of annual (B) SST (°C per kg/ha), (C) 200 hPa (upper) zonal wind (m/s per kg/ha), and (D) net OLR (W/m² per kg/ha). (E) Regression of detrended cacao–coffee yield (1976–2019) onto local fields of DJF seasonal (left–right) ERA5 surface zonal wind (m/s per kg/ha) and net solar radiation (W/m² per kg/ha), $N = 42$ yr; and (F) lag correlation function with index area detrended ERA5 zonal wind, evapotranspiration, soil moisture and solar radiation, where 0 refers to DJF season, shading covers insignificant values. In panels (B–E) lighter/darker shading refers to zones of weak/strong influence, insignificant values are masked using the KNMI climate explorer statistical analysis tool.

4. Conclusions

Elahi et al. [28] identify the risks to agriculture in the form of production, marketing, finance, the environment, and labor. Global-warming-induced extreme weather can increase these risks, motivating the need to offset harmful conditions through climate-sensitive farm management. This study has evaluated the winter (December–February) climate and the diurnal cycle of surface fluxes, boundary layer height, and landbreeze—trade wind confluence that underpins nocturnal convection over northeastern Dominican Republic, using a representative winter season (DJF17). Cool 15 °C air draining off the central mountains

meets incoming trade winds of 7–10 m/s within a shallow boundary layer from midnight to sunrise, creating a bow wave confluence along 70° W in longitude.

When a mid-latitude ridge joins the subtropical anticyclone, trade winds accelerate [4], and latent heat fluxes over the Atlantic moisten and deepen the marine layer along a 2000 km fetch that stirs large northeasterly waves. As the incoming trade winds approach the Dominican Republic at night, an opposing warm-to-cold thermal gradient slows and lifts the airflow, precipitating light rain over the Cibao Valley, where cacao and coffee are grown. Shallow clouds reach 40 dBz on windward slopes (cf. Figure 2E) but seldom overtop the mountains due to subsidence from the North Atlantic anticyclone during the winter.

A statistical regression of detrended annual cacao and coffee yields onto regional meteorological fields and local time series gave insights on how climate variability affects agricultural production from 1976–2019. Cooler sea temperatures and stronger trade winds during the winter favor higher cacao–coffee yields. Lag correlations between cacao–coffee yields and local evapotranspiration and solar radiation indicate that a cloudy autumn followed by a sunny spring help boost cash crop farming in the northeastern Dominican Republic. These parametric statistical methods were applied to monthly time series that have near-Gaussian distributions (cf. Appendix A). Agricultural risk managers could employ this knowledge to anticipate low yields following a negative NAO with warm sea temperatures, weak trade winds, and a dry autumn/wet spring condition. Further work will analyze hydrological responses and consider farming practices that could mitigate unfavorable climate signals.

Funding: This research received no external funding.

Data Availability Statement: Analyses are available on request via excel file.

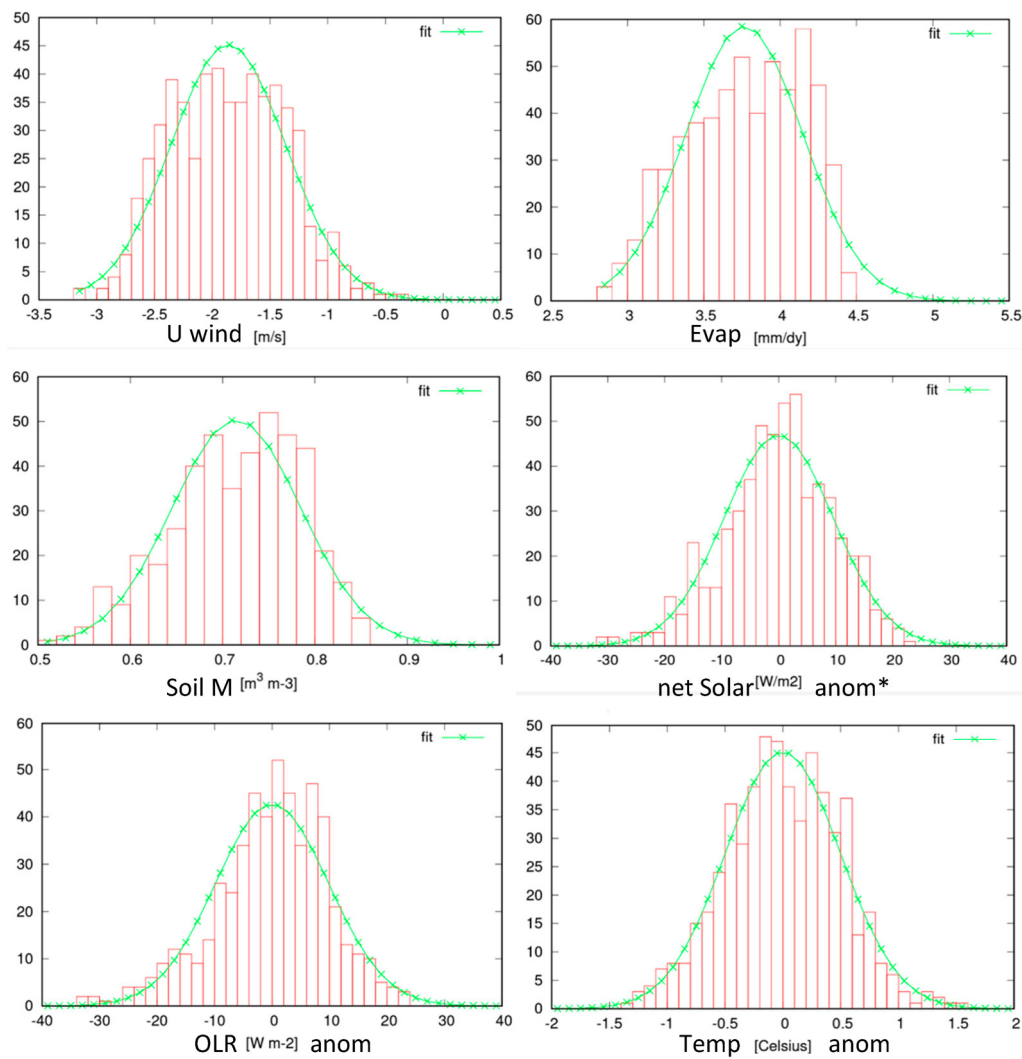
Acknowledgments: Website used in data analysis include IRI climate library, KNMI climate explorer, NASA giovanni, Univ Hawaii APDRC, NOAA ready ARL, NOAA Amdar, Univ Wyoming radiosonde, Univ Colorado CloudSat, and Iowa State Enviro Mesonet. All data are publicly available, and most methods employ the above websites to generate statistics and graphics, making the results eminently reproducible.

Conflicts of Interest: The authors declare no conflict of interest.

Appendix A

Histograms of monthly Cibao Valley meteorological time series used in statistical correlations, each fit with a Gaussian distribution (green) to evaluate outcomes. Y-axis refers to the number of months; ‘anom’ = departures from mean annual cycle. Statistics for one histogram are reported below.

Parameter	Value $\pm 2\sigma$	95% CI (W/m ²)
mean:	$0.79 \times 10^{-5} \pm 0.79$	−0.84...0.74
s.d. (n):	9.59 ± 0.58	8.99...10.15
s.d. (n − 1):	9.60	
skew:	-0.35 ± 0.18	−0.52...−0.16
min/max:	−31.58/23.15	
χ^2/df	52/31 = 1.67	$p = 0.011$



* Tabulated values for a gaussian fit to net Solar radiation anomalies, N = 564 months

References

1. Tobey, J.; Ortiz, A. Freshwater Flows to Estuaries and Water Budget of the Yuna River Watershed, Dominican Republic, USAID Report, Univ Rhode Island. 2004. Available online: <https://www.crc.uri.edu/> (accessed on 1 January 2022).
2. Jury, M.R.; Chiao, S. Meso-circulation associated with summer convection over the central Antilles. *Earth Int.* **2011**, *15*, 1–19. [CrossRef]
3. Perez, C.R.; Jury, M.R. Spatial and temporal analysis of climate change in Hispaniola. *Theor. Appl. Climatol.* **2013**, *113*, 213–224. [CrossRef]
4. Garcia, O.; Bosart, L.; DiMego, G. On the nature of the winter season rainfall in the Dominican Republic. *Mon. Weather Rev.* **1978**, *106*, 961–982. [CrossRef]
5. Martin, P.H.; Fahey, T.J. Mesoclimatic patterns shape the striking vegetation mosaic in the cordillera central, Dominican Republic. *Arct. Antarct. Alp. Res.* **2014**, *46*, 755–765. [CrossRef]
6. Izzo, M.; Aucelli, P.P.C.; Maratea, A. Historical trends of rain and air temperature in the Dominican Republic. *Int. J. Climatol.* **2021**, *41*, E563–E581. [CrossRef]
7. Jury, M.R. The pattern of climate change around the Windward Passage. *Theor. Appl. Climatol.* **2019**, *137*, 1149–1157. [CrossRef]
8. Jury, M.R. Resolution-dependent perspectives on Caribbean hydro-climate. *Hydrology* **2020**, *7*, 93. [CrossRef]
9. Herrera, D.A.; Mendez-Tejeda, R.; Centella-Artola, A.; Martínez-Castro, D.; Ault, T.; Delanoy, R. Projected hydroclimate changes on Hispaniola Island through the 21st Century in CMIP6 models. *Atmosphere* **2021**, *12*, 6. [CrossRef]
10. Payano-Almanzar, R.; Rodriguez, J. Meteorological, agricultural and hydrological drought in the Dominican Republic: A review. *Curr. World Environ.* **2018**, *13*, 124. [CrossRef]
11. DeAlmeida, A.-A.F.; Valle, R.R. Ecophysiology of the cacao tree. *Braz. J. Plant Physiol.* **2007**, *19*, 425–448. [CrossRef]

12. Lahive, F.; Hadley, P.; Daymond, A.J. The physiological responses of cacao to the environment and the implications for climate change resilience, a review. *Agron. Sustain. Dev.* **2019**, *39*, 5. [\[CrossRef\]](#)
13. Berlan, A.; Berges, A. Cocoa Production in the Dominican Republic, SCI Report Green-Black. 2013. Available online: <https://www.cocoalife.org/> (accessed on 1 January 2022).
14. DaMatta, F.M.; Ramalho, J.D.C. Effects of drought and temperature stress on coffee physiology and production: A review. *Braz. J. Plant Physiol.* **2006**, *18*, 55–81. [\[CrossRef\]](#)
15. DaMatta, F.M.; Ronchi, C.P.; Maestri, M.; Barros, R.S. Ecophysiology of coffee growth and production. *Braz. J. Plant Physiol.* **2007**, *19*, 485–510. [\[CrossRef\]](#)
16. Davis, A.P.; Gole, T.W.; Baena, S.; Moat, J. The impact of climate change on indigenous Arabica coffee: Predicting future trends and identifying priorities. *PLoS ONE* **2012**, *7*, e47981. [\[CrossRef\]](#)
17. Siegel, P.B.; Alwang, J. Export Commodity Production and Broad-Based Rural Development: Coffee and Cocoa in the Dominican Republic, World Bank Policy Res Paper 3306. 2004. Available online: <https://econ.worldbank.org> (accessed on 1 January 2022).
18. Food and Agriculture Organization. Cacao and Coffee Yield Data for the Dominican Republic. 2021. Available online: <https://www.fao.org/faostat/en/#data/QC> (accessed on 1 January 2022).
19. Izzo, M.; Rosskopf, C.M.; Aucelli, P.P.C.; Maratea, A.; Méndez, R.; Pérez, C.; Segura, H. A new climatic map of the Dominican Republic based on the Thornthwaite classification. *Phys. Geogr.* **2010**, *31*, 455–472. [\[CrossRef\]](#)
20. Funk, C.C.; Peterson, P.J.; Landsfeld, M.F.; Pedreros, D.H.; Verdin, J.P.; Rowland, J.D.; Romero, B.E.; Husak, G.J.; Michaelsen, J.C.; Verdin, A.P. A quasi-global precipitation time series for drought monitoring. *U.S. Geol. Surv. Data Ser.* **2014**, *832*, 4. [\[CrossRef\]](#)
21. Hou, A.Y.; Kakar, R.K.; Neeck, S.; Azarbarzin, A.; Kummerow, C.D.; Kojima, M.; Oki, R.; Nakamura, K.; Iguchi, T. The Global Precipitation Measurement mission. *Bull. Am. Meteorol. Soc.* **2014**, *95*, 701–722. [\[CrossRef\]](#)
22. Saha, S.; Moorthi, S.; Wu, X.; Wang, J.; Nadiga, S.; Tripp, P.; Behringer, D.; Hou, Y.T.; Chuang, H.Y.; Iredell, M.; et al. The NCEP climate forecast system version 2. *J. Clim.* **2014**, *27*, 2185–2208. [\[CrossRef\]](#)
23. Hersbach, H.; Bell, B.; Berrisford, P.; Hirahara, S.; Horányi, A.; Muñoz-Sabater, J.; Nicolas, J.; Peubey, C.; Radu, R.; Schepers, D.; et al. The ERA5 global reanalysis. *Q. J. R. Meteorol. Soc.* **2020**, *146*, 1999–2049. [\[CrossRef\]](#)
24. Janjic, Z.I. A nonhydrostatic model based on a new approach. *Meteorol. Atmos. Phys.* **2003**, *82*, 271–285. [\[CrossRef\]](#)
25. Chassignet, E.P.; Hurlburt, H.E.; Metzger, E.J.; Smedstad, O.M.; Cummings, J.A.; Halliwell, G.R.; Bleck, R.; Baraille, R.; Wallcraft, A.J.; Lozano, C.; et al. US GODAE: Global ocean prediction with the Hybrid coordinate ocean model (HYCOM). *Oceanography* **2009**, *22*, 64–75. [\[CrossRef\]](#)
26. Tolman, H.L.; Balasubramanian, B.; Burroughs, L.D.; Chalikov, D.V.; Chao, Y.Y.; Chen, H.S.; Gerald, V.M. Development and implementation of wind generated ocean surface wave models at NCEP. *Weather Forecast* **2002**, *17*, 311–333. [\[CrossRef\]](#)
27. Martinez, C.; Kushnir, Y.; Goddard, L.; Ting, M. Interannual variability of the early and late-rainy seasons in the Caribbean. *Clim. Dyn.* **2020**, *55*, 1563–1583. [\[CrossRef\]](#)
28. Elahi, E.; Khalid, Z.; Tauni, M.Z.; Zhang, H.; Lirong, X. Extreme weather events risk to crop-production and the adaptation of innovative management strategies to mitigate the risk: A retrospective survey of rural Punjab, Pakistan. *Technovation* **2022**, *117*, 102255. [\[CrossRef\]](#)

Disclaimer/Publisher’s Note: The statements, opinions and data contained in all publications are solely those of the individual author(s) and contributor(s) and not of MDPI and/or the editor(s). MDPI and/or the editor(s) disclaim responsibility for any injury to people or property resulting from any ideas, methods, instructions or products referred to in the content.